JACS
JOURNAL OF THE AMERICAN CHEMICAL SOCIETY
Communication
pubs.acs.org/JACS

# Molecular Engineering To Control the Magnetic Interaction between Single-Chain Magnets Assembled in a Two-Dimensional Network

Luminita M. Toma,[†] Catalina Ruiz-Pérez,[‡] Jorge Pasán,[‡] Wolfgang Wernsdorfer,[§] Francesc Lloret,[†] and Miguel Julve*,[†]

[†]Instituto de Ciencia Molecular, University of Valencia, Catedrático José Beltrán 2, 46980 Paterna, Valencia, Spain

[‡]Laboratorio de Rayos X y Materiales Moleculares, Departamento de Física Fundamental II, Facultad de Física, Universidad de la Laguna, Avda. Astrofísico Francisco Sánchez s/n, 38204 La Laguna, Tenerife, Spain

[§]Nanoscience Department, Institut Néel, CNRS, BP 166, 25 Avenue des Martyrs, 380412 Grenoble Cedex 9, France

Supporting Information

**ABSTRACT:** Two two-dimensional (2D) systems having the formula $[\{Fe^{III}(dmbpy)(CN)_4\}_2Co^{II}L]_n$ [L = pyetNO (**1**), tvpNO (**2**)] and consisting of single-chain magnets connected through organic ligands (L) have been prepared, and their magnetic properties have been investigated. The overall magnetic behavior depends on the capacity of the organic pillars to transmit long-range magnetic interactions. **1** is the first example of a 2D compound exhibiting double relaxation of the magnetization, whereas **2** behaves as a metamagnet.

Single-chain magnets (SCMs) are attractive research targets of polymeric molecular materials displaying slow relaxation of the magnetization and hysteresis effects.[1−11] Because of their fascinating fundamental nature and potential applications as ultimate memory or quantum spintronic devices, increased synthetic efforts were devoted to obtaining such 1D compounds in the past decade. Their synthesis is a current challenge in which achieving strong uniaxial (Ising) anisotropy and minimizing the interchain magnetic interactions are essential requirements.[12] While anisotropy could be achieved by the choice of an appropriate metal ion such as high-spin octahedral Co(II),[4,5,9b,c,10,11] Mn(III),[2b−f,6,8,9a] Fe(II),[2a] or Re(IV),[3] the tuning of the intermolecular interactions between magnetic nanowires to maintain a sufficiently large ratio of intra- to interchain magnetic interactions is a more complicated task because of the inherent difficulties in controlling the crystal packing. Several ways to avoid intermolecular magnetic interactions have been proposed, including the introduction of bulky ligands between/within the chains[1d,10d,13] and the use of H-bonding nucleobase groups[2f] or even structurally ditopic, magnetically inert organic linkers[14] that would allow the ferro- or ferrimagnetic Ising chains to be linked into 2D or 3D networks without significant changing the SCM behavior.

As an extension of these strategies, we present here a new way to obtain SCMs by controlling not only the interchain separation but also the arrangement of the chains in the crystal packing and the magnetic interactions between the magnetic nanowires. We incorporate bulky substituents in the cyanide-bearing precursor in addition to the use of organic spacers to afford 2D networks. Within each layer, the choice of the appropriate extended spacer allows the control of the interchain interactions, freezing the magnetization in one direction. Moreover, the bulky ligands present within each chain preclude any interaction between the neighboring 2D networks. In a very recent work,[10d] we showed how the use of the sterically hindered cyanide-bearing low-spin Fe(III) complex $[Fe(dmbpy)(CN)_4]^-$ (dmbpy = 4,4′-dimethyl-2,2′-bipyridine) as a ligand toward fully solvated Co(II) ions afforded the 4,2-wavelike $[\{Fe^{III}(dmbpy)(CN)_4\}_2Co^{II}(H_2O)_2]_n\cdot 4nH_2O$ ferromagnetic chain that exhibits an unprecedented double slow relaxation of the magnetization. A close-up of the structure shows sixfold-coordinated Co(II) ions with two water molecules in trans positions (Scheme 1).

**Scheme 1. Schematic View of the Formation of 1 and 2**[a]

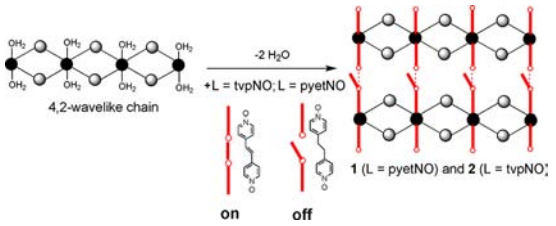


[a]The coordinated water molecules in the 1D compound are substituted by organic ligands that act as ON/OFF pathways for the interchain magnetic interactions.

In this work, we show how the exo bis-monodentate organic linkers 1,2-bis(4-pyridyl)ethane-*N*,*N*′-dioxide (pyetNO) and 1,2-bis(4-pyridyl)ethylene-*N*,*N*′-dioxide (tvpNO) can replace the water molecules coordinated to the Co(II) ion to afford 2D networks in which the overall magnetic behavior depends on the capacity of the organic pillars to transmit long-range magnetic interactions (Scheme 1).

The reaction of $[Co(L)_2(NO_3)_2]$ with $PPh_4[Fe(dmbpy)(CN)_4]\cdot 2H_2O$ in an acetonitrile/water mixture afforded X-ray-quality crystals of $[\{Fe^{III}(dmbpy)(CN)_4\}_2Co^{II}L]_n$ with L = pyetNO (**1**) or tvpNO (**2**). **1** and **2** are isostructural compounds. A fragment of the structure of **2** is shown in

**Received:** July 23, 2012
**Published:** September 6, 2012

   dx.doi.org/10.1021/ja307042z | J. Am. Chem. Soc. 2012, 134, 15265−15268

Figure 1 (see Figure S1 in the Supporting Information for the structure of **1**). The structure contains neutral layers consisting

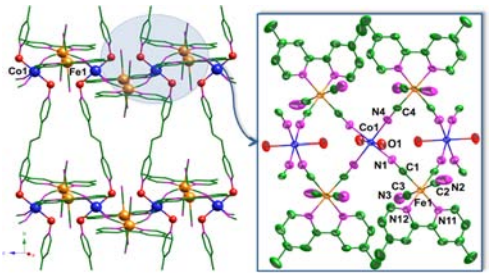


**Figure 1.** Fragment of the 2D structure of **2** (left) made of neutral chains (right) interlinked through *trans*-tvpNO ligands.

of 4,2-wavelike $[\{Fe(dmbpy)(CN)_4\}_2Co]$ chains running parallel to the crystallographic *c* axis that are connected through *anti*-pyetNO (**1**) and *trans*-tvpNO (**2**) molecules acting as bis-monodentate ligands. These layers are further stacked along the crystallographic *b* axis through van der Waals interactions with a shortest interlayer Fe1···Fe1(a) distance of 6.639(2) (**1**) and 6.653(2) Å (**2**) [symmetry code: (a) = $x, -y, z + {}^1/_2$] (Figure S2).

Within each chain, each $[Fe^{III}(dmbpy)(CN)_4]^-$ entity acts as a bis-monodentate ligand toward *trans*-$[Co^{II}L]$ units through two of its four cyanide nitrogens in the cis position, affording neutral 4,2-wavelike $[\{Fe^{III}(dmbpy)(CN)_4\}_2Co^{II}L]$ 1D motifs. The bidentate dmbpy molecule and the two bridging cyanide ligands are located in the equatorial plane of the iron(III) ion, inducing a quasi-planar alignment between the nearest aromatic dmbpy ligands. To avoid steric constraints between the methyl groups of adjacent dmbpy molecules, the whole skeleton of the chain twists to adopt a wavelike shape. The values of the iron−cobalt separation across the bridging cyanide ligands in **1** and **2** vary in the narrow range 4.9822(12)−5.0596(5) Å. The iron atoms in **1** and **2** exhibit a somewhat distorted $FeC_4N_2$ octahedral environment, the main source of the distortion being the reduced bite of the chelating dmbpy ligand [N11−Fe1−N12 = 80.8(3)° in **1** and 79.4(5)° in **2**]. The bond lengths and angles in the $[Fe(dmbpy(CN)_4]$ fragment [Fe1−N = 1.935(10)−1.997(11) Å and Fe1−C = 1.888(13)−1.967(11) Å] agree with those reported for the low-spin iron(III) complex $PPh_4[Fe(dmbpy)(CN)_4]\cdot 3H_2O$ [Fe−N = 1.99 Å and Fe−C = 1.91−1.96 Å].[10d] Each cobalt atom in **1** and **2** is sixfold-coordinated, with four equatorial cyanide nitrogen atoms [Co1−N = 2.082(7) and 2.100(7) Å in **1** and 2.069(11) and 2.086(11) Å in **2**] and two axial pyridine oxide oxygens [Co1−O = 2.098(6) Å in **1** and 2.120(9) Å in **2**]. Pairs of crystallographically related $Co^{II}$ ions from two neighboring chains are bridged through one *anti*-$\mu$-*O*,*O*′-pyetNO in **1** and *trans*-$\mu$-*O*,*O*′-tvpNO in **2**, with interchain cobalt−cobalt distances of 14.15 Å in **1** and 14.21 Å in **2**.

The temperature dependence of the $\chi_M T$ product per $Fe^{III}_2Co^{II}$ unit for **1** (Figure S3) at 120 K is 4.44 $cm^3\ mol^{-1}$ K, in agreement with the presence of two magnetically noninteracting low-spin iron(III) centers and one high-spin cobalt(II) ion with large spin−orbit contributions. Upon cooling, $\chi_M T$ smoothly increases as *T* decreases to ca. 20 K and then exhibits a sharp increase for $T < 20$ K, reaching a maximum value of 294.4 $cm^3\ mol^{-1}$ K at 4.0 K; this is followed by a decrease to 115.6 $cm^3\ mol^{-1}$ K at 1.9 K. $\chi_M T$ decreases linearly with *T* at very low temperatures as the magnetization ($M$) becomes field-dependent. The plot of $M$ per $Fe^{III}_2Co^{II}$ unit versus applied field ($H$) at 2.0 K reaches a value of 4.30 $\mu_B$ at 5 T (Figure S3 inset). These features indicate the occurrence of a ferromagnetic interaction between the low-spin iron(III) and high-spin cobalt(II) ions across the bridging cyanide. Hysteresis loops were observed only below 2.0 K which are dependent on the temperature and field sweep rate (Figures S4 and S5, respectively).

Alternating-current (ac) magnetic susceptibility measurements for **1** at different frequencies exhibit temperature dependence of the in-phase ($\chi'_M$) and out-of-phase ($\chi''_M$) components (Figure S6). Curiously, two frequency-dependent out-of-phase ac peaks were observed in the temperature ranges 3.0−4.0 and 2.0−3.0 K The partial overlap of the two families of peaks precluded an accurate evaluation of the blocking temperature (which is given by the maximum of $\chi''_M$), and then the estimation of the values of the relaxation time $\tau_0$ and the barrier for the magnetization reversal ($E_a/k_B$) through the Arrhenius equation. To analyze the dynamics of the magnetization relaxation for **1**, ac isotherms at different frequencies were measured and drawn as Argand diagrams (Figure 2). The

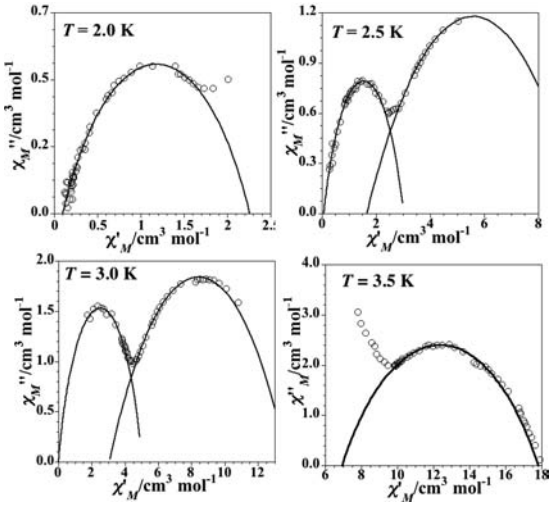


**Figure 2.** Argand diagrams for **1** at different temperatures. The solid lines are the least-squares fits obtained using the Cole−Cole model (see the text).

presence of two flattened semicircles for the same temperature (2.5 and 3.0 K) gives us a hint that two relaxation processes are involved. To our knowledge, this is the first time that two different relaxation processes describing two independent semicircles in an Argand plot has been observed in a structurally characterized 2D system whose magnetic behavior is one of a SCM (very recent examples concerning 1D systems have been found previously by our group).[4c,10d] The fit of the data through the Cole−Cole method[15] by considering two relaxation processes separately led to values of 0.43 (2.0 K), 0.36 and 0.62 (2.5 K), 0.30 and 0.58 (3.0 K), and 0.47 (3.5 K) for the parameter $\alpha$, which determines the width of the $\tau$ distribution. This indicates that each of the relaxation process is characterized by a distribution of relaxation times.[10c] Also, $\alpha$ increases as the temperature decreases, following the enhancement of the intermolecular interactions. From the maximum of $\chi''_M$, we calculated the following values for the relaxation time [$\tau = (2\pi\nu)^{-1}$]: 0.08 (2.0 K), $2.89 \times 10^{-3}$ and 3.18 (2.5 K), $2.2 \times 10^{-4}$ and 0.2 (3.0 K), and $5.3 \times 10^{-3}$ s (3.5 K). With the three


dx.doi.org/10.1021/ja307042z | J. Am. Chem. Soc. 2012, 134, 15265−15268

calculated values of $\tau$ for each of the relaxation processes, the values of $\tau_0$ and $E_a$ were estimated as $\tau_0 = 1.9 \times 10^{-9}$ s and $E_a$ = 24.5 $cm^{-1}$ for one relaxation process and $\tau_0 = 1.15 \times 10^{-9}$ s and $E_a$ = 38.3 $cm^{-1}$ for the other. At lower temperatures, the relaxation rate was too slow for ac magnetic susceptibility measurements, and we used relaxation measurements with the micro-SQUID technique[16] in the temperature range 0.6 K $\leq T \leq$ 2.1 K (Figure S7) to extract the relaxation time. Because the decay is not exponential, a scaling procedure allowed us to get the mean relaxation time, and the Arrhenius plot (Figure S8) showed two regimes with a crossover at 1.7 K, which is interpreted as the manifestation of finite-size effects.[17]

At room temperature, the value of $\chi_M T$ per $Fe^{III}_2Co^{II}$ unit of **2** is 4.13 $cm^3$ $mol^{-1}$ K, as expected for two low-spin iron(III) and one high-spin cobalt(II) isolated ions with significant orbital contributions. Upon cooling, $\chi_M T$ smoothly increases in a monotonic way until $T$ reaches 50 K, in line with an intrachain ferromagnetic coupling between the Co(II) and Fe(III) ions, and then a maximum of 13.6 $cm^3$ $mol^{-1}$ K is rapidly achieved at 8.0 K; $\chi_M T$ then decreases to 0.25 $cm^3$ $mol^{-1}$ K at 1.9 K (Figure 3). A maximum in the magnetic

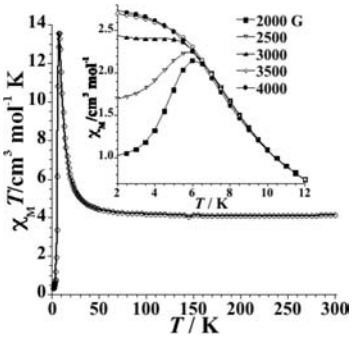


**Figure 3.** $\chi_M T$ vs $T$ plot for **2** under an applied magnetic field of 1000 G ($T \geq$ 30 K) and 100 G ($T <$ 30 K). Inset: field dependence of $\chi_M$ in the low-temperature region.

susceptibility was observed at ca. 6.0 K for applied fields lower than 3000 G (Figure 3 inset). This maximum disappeared for $H >$ 3000. These features, together with the sigmoidal shape of the $M$ versus $H$ plot at 2.0 K (Figure 4), prove the occurrence of a weak antiferromagnetic coupling between the ferromagnetic chains, which is overcome by an applied direct-current (dc) field above 3000 G.

This metamagnetic-like behavior is consistent with the structure of **2**, with ferromagnetic $Fe^{III}_2Co^{II}$ chains interacting in an antiparallel way between them through the *trans*-tvpNO

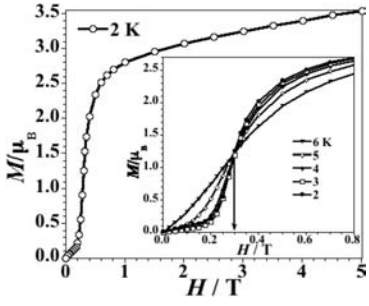


**Figure 4.** $M$ vs $H$ plot for **2** at 2.0 K. Inset: $M$ vs $H$ isotherms (2.0 $\leq T \leq$ 6.0 K).

ligands. The $\pi$-type orbital pathways through the aromatic pyridyl-containing bridges could be the origin for this exchange interaction. The magnetic energy for $H$ = 3000 G is ca. 0.3 $cm^{-1}$, a value which roughly corresponds to the interchain antiferromagnetic interaction. Under this magnetic field, the resulting noninteracting ferromagnetic anisotropic $Fe^{III}_2Co^{II}$ chains show slow relaxation of the magnetization as well as frequency dependence of $\chi'_M$ and $\chi''_M$ (Figure 5).

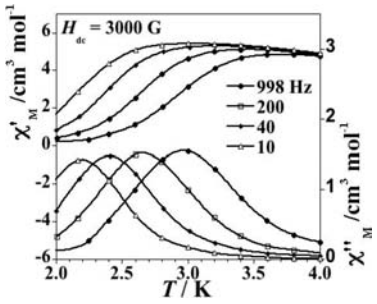


**Figure 5.** Thermal dependence of the (top) $\chi'_M$ and (bottom) $\chi''_M$ components of the ac magnetic susceptibility of **2** under an oscillating field of 1 G ($\nu$ = 10−1000 Hz) and an applied field of 3000 G.

The Cole−Cole plots for **2** at 2.0 and 3.0 K follow the shape of a semicircle characteristic of a single relaxation process (Figure S9). The theoretical curves obtained by least-squares fits of the experimental data for **2** using a generalized Debye model reproduced the observed semicircles (solid lines in Figure S9) and provided $\alpha$ values of 0.34 ($T$ = 3.0 K) and 0.44 ($T$ = 2.0 K), which are somewhat greater than that expected for an SCM ($\alpha$ = 0 for an ideal Debye model with a single relaxation time); in general, these are values commonly attributed to the existence of interchain magnetic interactions ($0 < \alpha < 0.5$). The increase in these interactions with decreasing temperature accounts for the increase in $\alpha$ as $T$ goes from 3.0 to 2.0 K. To study the relaxation of the magnetization at very low temperatures, $M$ versus $H$ (temperature range 0.04−1.5 K) (Figure S10) as well as time-dependent magnetization (Figure S11) micro-SQUID measurements were done. The $M$ vs $H$ plot at 1.5 K exhibits a sigmoidal shape similar to that observed at higher temperatures in the SQUID measurements. However, a small hysteresis occurs, which increases while the sigmoidal curve disappears with decreasing temperature, leading to a squared loop similar to that of a ferromagnet. The fact that the remnant magnetization at $H$ = 0 G in the very low temperature domain is the same as that expected for the saturation magnetization of the ferromagnetically ordered chain suggests that the relaxation of the chains from parallel to antiparallel spin arrangements is very small when the applied magnetic field is removed. Thus, the $M$ versus time plot shown in Figure S11 constitutes a measure of this interchain relaxation. Figure S12 shows the Arrhenius law for this relaxation (red circles) compared with the relaxation of the chain in the presence of an applied magnetic field (green squares). One can see that the intra- and interchain regimes are different (in contrast to what is observed for **1**). The interchain relaxation shows also two regimes: (i) above 1.3 K, the thermal dependence of the relaxation time follows an Arrhenius law with $E_a$ = 33.9 $cm^{-1}$ and $\tau_0 = 1.5 \times 10^{-14}$ s; (ii) below 1.3 K, a smaller activation energy of 11.3 $cm^{-1}$ and a $\tau_0 = 1.8 \times 10^{-4}$ s is found.


dx.doi.org/10.1021/ja307042z | J. Am. Chem. Soc. 2012, 134, 15265−15268

It deserves to be noted that the intrachain relaxation is slower than the interchain one over the whole temperature range (Figure S13). Thus, one can consider that the magnetization within each chain at low temperature is blocked, and the decrease in the magnetization observed in the dc measurements (under zero applied magnetic field) have to be attributed to the change from a ferromagnetic spin arrangement between the chains to an antiferromagnetic one.

## ■ ASSOCIATED CONTENT

### Supporting Information

Experimental details; structural data, including CIF files for **1** and **2**; and additional magnetic data. This material is available free of charge via the Internet at http://pubs.acs.org.

## ■ AUTHOR INFORMATION


### Corresponding Author

Miguel.Julve@uv.es


### Notes

The authors declare no competing financial interest.

## ■ ACKNOWLEDGMENTS

This work was supported by the Ministerio Español de Ciencia e Innovación (Projects CTQ2010-15364, MAT2010-16891, CSD2007-00010, and DPI 2010-21103-CO4-O3) and the Generalitat Valenciana (PROMETEO/2009/108 and ISIC2012/002).

## ■ REFERENCES


(1) (a) Lescouëzec, R.; Toma, L. M.; Vaissermann, J.; Verdaguer, M.; Delgado, F. S.; Ruiz-Pérez, C.; Lloret, F.; Julve, M. *Coord. Chem. Rev.* **2005**, *249*, 2691. (b) Bogani, L.; Vindigni, A.; Sessoli, R.; Gatteschi, D. *J. Mater. Chem.* **2008**, *18*, 4750. (c) Vindigni, A. *Inorg. Chim. Acta* **2008**, *361*, 3731. (d) Miyasaka, H.; Julve, M.; Yamashita, M.; Clérac, R. *Inorg. Chem.* **2009**, *48*, 3420. (e) Sun, H. L.; Wang, Z. M.; Gao, S. *Coord. Chem. Rev.* **2010**, *254*, 1081.

(2) (a) Kajiwara, T.; Nakano, M.; Kaneko, Y.; Takaishi, S.; Ito, T.; Yamashita, M.; Igashira-Kamiyama, A.; Nojiri, H.; Ono, Y.; Kojima, N. *J. Am. Chem. Soc.* **2005**, *127*, 10150. (b) Miyasaka, H.; Madanbashi, T.; Sugimoto, K.; Nakazawa, Y.; Wernsdorfer, W.; Sugiura, K.-i.; Yamashita, M.; Coulon, C.; Clérac, R. *Chem.—Eur. J.* **2006**, *12*, 7028. (c) Miyasaka, H.; Saitoh, A.; Yamashita, M.; Clérac, R. *Dalton Trans.* **2008**, 2422. (d) Miyasaka, H.; Takayama, K.; Saytoh, A.; Furukawa, S.; Yamashita, M.; Clérac, R. *Chem.—Eur. J.* **2010**, *16*, 3656. (e) Miyasaka, H.; Madanbashi, T.; Saytoh, A.; Motokawa, N.; Ishikawa, R.; Yamashita, M.; Bahr, S.; Wernsdorfer, W.; Clérac, R. *Chem.—Eur. J.* **2012**, *18*, 3942. (f) Zhang, W. X.; Shiga, T.; Miyasaka, H.; Yamashita, M. *J. Am. Chem. Soc.* **2012**, *134*, 6908.

(3) (a) Harris, T. D.; Bennett, M. V.; Clérac, R.; Long, J. R. *J. Am. Chem. Soc.* **2011**, *132*, 3980. (b) Feng, X.; Harris, T. D.; Long, J. R. *Chem. Sci* **2011**, *2*, 1688. (c) Feng, X.; Liu, J.; Harris, T. D.; Hill, S.; Long, J. R. *J. Am. Chem. Soc.* **2012**, *134*, 7521.

(4) (a) Pardo, E.; Ruiz-García, R.; Lloret, F.; Faus, J.; Julve, M.; Journaux, Y.; Novak, M. A.; Delgado, F. S.; Ruiz-Pérez, C. *Chem.—Eur. J.* **2007**, *13*, 2054. (b) Pardo, E.; Train, C.; Lescouëzec, R.; Journaux, Y.; Pasán, J.; Ruiz-Pérez, C.; Delgado, F. S.; Ruiz-García, R.; Lloret, F.; Paulsen, C. *Chem. Commun.* **2010**, *46*, 2322. (c) Ferrando-Soria, J.; Pardo, E.; Ruiz-García, R.; Cano, J.; Lloret, F.; Julve, M.; Journaux, Y.; Pasán, J.; Ruiz-Pérez, C. *Chem.—Eur. J.* **2011**, *17*, 2176. (d) Ferrando-Soria, J.; Cangussu, D.; Eslava, M.; Journaux, Y.; Lescouëzec, R.; Julve, M.; Lloret, F.; Pasán, J.; Ruiz-Pérez, C.; Lhotel, E.; Paulsen, C.; Pardo, E. *Chem.—Eur. J.* **2011**, *17*, 12482.

(5) (a) Coronado, E.; Galán-Mascarós, J. R.; Martí-Gastaldo, C. *J. Am. Chem. Soc.* **2008**, *130*, 14987. (b) Coronado, E.; Galán-Mascarós, J. R.; Martí-Gastaldo, C. *CrystEngComm* **2009**, *11*, 2143.

(6) Bernot, K.; Luzon, J.; Sessoli, R.; Vindigni, A.; Thion, J.; Richeter, S.; Leclercq, D.; Larionova, J.; van der Lee, A. *J. Am. Chem. Soc.* **2008**, *130*, 1619.

(7) Costes, J. P.; Vendier, L.; Wernsdorfer, W. *Dalton Trans.* **2010**, *39*, 4886.

(8) Ruiz, R.; Castro, I.; Pardo, E.; Ferrando-Soria, J.; Cano, J.; Lloret, F.; Julve, M. *J. Braz. Chem. Soc.* **2011**, *22*, 974.

(9) (a) Bai, Y. L.; Tao, J.; Wernsdorfer, W.; Sato, O.; Huang, R. B.; Zheng, L. S. *J. Am. Chem. Soc.* **2006**, *128*, 16428. (b) Liu, T.; Zhang, Y. J.; Kanegawa, S.; Sato, O. *J. Am. Chem. Soc.* **2010**, *132*, 8250. (c) Dong, D. P.; Liu, T.; Kanegawa, S.; Kang, S.; Sato, O.; He, C.; Duan, C. Y. *Angew. Chem., Int. Ed.* **2012**, *51*, 5119.

(10) (a) Toma, L. M.; Lescouëzec, R.; Lloret, F.; Julve, M.; Vaissermann, J.; Verdaguer, M. *Chem. Commun.* **2003**, 1850. (b) Lescouëzec, R.; Vaissermann, J.; Ruiz-Pérez, C.; Lloret, F.; Carrasco, R.; Julve, M.; Verdaguer, M.; Dromzée, Y.; Gatteschi, D.; Wernsdorfer, W. *Angew. Chem., Int. Ed.* **2003**, *42*, 1483. (c) Toma, L. M.; Lescouëzec, R.; Pasán, J.; Ruiz-Pérez, C.; Vaissermann, J.; Cano, J.; Carrasco, R.; Wernsdorfer, W.; Lloret, F.; Julve, M. *J. Am. Chem. Soc.* **2006**, *128*, 4842. (d) Toma, L. M.; Ruiz-Pérez, C.; Lloret, F.; Julve, M. *Inorg. Chem.* **2012**, *51*, 1216.

(11) Caneschi, A.; Gatteschi, D.; Lalioti, N.; Sangregorio, C.; Sessoli, R.; Venturi, G.; Vindigni, A.; Rettori, A.; Pini, M. G.; Novak, M. A. *Angew. Chem., Int. Ed.* **2001**, *40*, 1760.

(12) Glauber, R. J. *J. Math. Phys.* **1963**, *4*, 294.

(13) Bogani, L.; Sangregorio, C.; Sessoli, R.; Gatteschi, D. *Angew. Chem., Int. Ed.* **2005**, *44*, 5817.

(14) Zheng, Y. Z.; Tong, M. L.; Zhang, W. X.; Chen, X. M. *Angew. Chem., Int. Ed.* **2008**, *45*, 6310.

(15) Cole, K. S.; Cole, R. H. *J. Chem. Phys.* **1941**, *9*, 341.

(16) Wernsdorfer, W. *Adv. Chem. Phys.* **2001**, *118*, 99.

(17) Wernsdorfer, W.; Murugescu, M.; Tasiopoulos, A. J.; Christou, G. *Phys. Rev. B* **2005**, *72*, No. 212406.